Atmospheric Research 280 (2022) 106434

Contents lists available at ScienceDirect

Atmospheric Research

journal homepage: www.elsevier.com/locate/atmosres

Dynamics of the Atmospheric Boundary Layer over two middle-latitude rural sites with Doppler lidar

Pablo Ortiz-Amezcua [a,b], Juana Andújar-Maqueda [b,c], Antti J. Manninen [d], Pyry Pentikäinen [e], Ewan J. O'Connor [d,f], Iwona S. Stachlewska [a], Gregori de Arruda Moreira [g], José Antonio Benavent-Oltra [b,h], Juan Andrés Casquero-Vera [b,c,e], Patryk Poczta [i,j], Dongxiang Wang [k], Kamila M. Harenda [i], Bogdan H. Chojnicki [i], Dominika M. Szczepanik [a], Łucja Janicka [a], Dirk Schüttemeyer [l], Lucas Alados-Arboledas [b,c], Juan Luis Guerrero-Rascado [b,c,*]

[a] Faculty of Physics, University of Warsaw (IGFUW), Warsaw, Poland
[b] Andalusian Institute for Earth System Research (IISTA-CEAMA), Granada, Spain
[c] Department of Applied Physics, University of Granada, Spain
[d] Finnish Meteorological Institute, Helsinki, Finland
[e] Institute for Atmospheric and Earth System Research (INAR)/Physics, Faculty of Science, University of Helsinki, Helsinki, Finland
[f] Department of Meteorology, University of Reading, United Kingdom
[g] Astronomy, Geophysics and Atmospheric Science Institute, University of São Paulo, São Paulo, Brazil
[h] Department of Electrical, Electronical and Automatic Control Engineering and Applied Physics, Escuela Técnica Superior de Ingeniería y Diseño Industrial, Universidad Politécnica de Madrid, Spain
[i] Laboratory of Bioclimatology, Poznan University of Life Sciences, Poznan, Poland
[j] Department of Grassland and Natural Landscape Sciences, Faculty of Agronomy and Bioengineering, Poznan University of Life Sciences, Poznan, Poland
[k] SEPCOIII Electric Power Construction Co., Ltd., Qingdao 266100, China
[l] European Space Research and Technology Centre, European Space Agency (ESA), Noordwijk, the Netherlands

ARTICLE INFO

Keywords:
Doppler lidar
Wind
Turbulence
Rural boundary layer
Olive orchard
Peatland

ABSTRACT

The Atmospheric Boundary Layer (ABL) over two middle-latitude rural sites was characterized in terms of mean horizontal wind and turbulence sources using a standard classification methodology based on Doppler lidar. The first location was an irrigated olive orchard in Úbeda (Southern Spain), representing one of the most important crops in the Mediterranean basin and a typical site with Mediterranean climate. The second location was PolWET peatland site in Rzecin (Northwestern Poland), representing one of the largest natural terrestrial carbon storages that have a strong interaction with the climate system. The results showed typical situations for non cloud-topped ABL cases, where ABL is fully developed during daytime due to convection, with high turbulent activity and strong positive skewness indicating frequent and powerful updrafts. The cloud-topped cases showed the strong influence that clouds can have on ABL development, preventing it to reach the same maximum height and introducing top-down movements as an important contribution to mixing. The statistical analysis of turbulent sources allowed for finding a common diurnal cycle for convective mixing at both sites, but nocturnal wind shear driven turbulence with marked differences in its vertical distribution. This analysis demonstrates the Doppler lidar measurements and the classification algorithm strong potential to characterize the dynamics of ABL in its full extent and with high temporal resolution. Moreover, some recommendations for future improvement of the classification algorithm were provided on the basis of the experience gained.

1. Introduction

The Atmospheric Boundary Layer (ABL) is the closest atmospheric layer to the Earth's surface, directly influenced by surface-atmosphere exchanges of moisture, heat, and other constituents, due to the impact from the biosphere and anthropogenic activities (Cimini et al., 2020).

* Corresponding author at: Andalusian Institute for Earth System Research (IISTA-CEAMA), Granada, Spain.
E-mail address: rascado@ugr.es (J.L. Guerrero-Rascado).

https://doi.org/10.1016/j.atmosres.2022.106434
Received 27 April 2022; Received in revised form 5 September 2022; Accepted 5 September 2022
Available online 8 September 2022

The characterization of this layer under different conditions is important not only for weather and climate models (Illingworth et al., 2016), but also for wind energy applications (e.g. Gökçek et al., 2007; Li and Yu, 2017) and air quality studies (e.g. Bossioli et al., 2009). The definition of the extent of this layer is still ambiguous and depends on the tracers and criteria chosen (e.g. temperature, aerosol concentration, or turbulence), although there have been recent efforts to harmonise and standardise such criteria in the framework of European programs developed in the last decade, such as the Cost Actions TOPROF and PROBE (Cimini et al., 2020; Kotthaus et al., 2022). One of the most important features that makes ABL description complex is the turbulent mixing, responsible for the redistribution of momentum, mass, temperature and humidity within this layer (Oke, 1992). The sources of turbulent mixing exhibit significant temporal and spatial variations, and include buoyancy (that produces upwards convective mixing), wind shear (mechanical mixing) or radiative cooling in stratocumulus clouds (producing top-down convective mixing).

In this context, lidar technique represents a powerful tool to retrieve profiles of several ABL properties as aerosol properties, temperature, wind or humidity. In particular, Doppler lidars (those measuring the Doppler shift due to the movement of aerosol particles by the wind) are used to retrieve the 3D wind field inside the ABL and to retrieve turbulent properties with high temporal and vertical resolution, which can be combined to classify turbulence basing on its source (Manninen et al., 2018). Manninen (2019b) developed 'Halo lidar toolbox', a software package with the aim of providing a robust tool to produce harmonized Doppler lidar retrievals applied to measurements from different sites using methods presented in peer-reviewed articles. In the present work, we use that standard and objective tool and classification methodology to characterize ABL in different locations and situations.

In particular, we characterized the ABL over two experimental rural sites with different features in terms of mean horizontal wind and turbulence sources. The detailed knowledge and study of the ABL dynamics over rural ecosystems is of high importance, among other reasons, and because of the role of wind and turbulence for ventilation processes and potential release of stored CO_2 (e.g. Bowling and Massman, 2011; Nachshon et al., 2012; Rey et al., 2012; Sánchez-Cañete et al., 2016) or because wind is a key factor in dispersion of pollen grains and other bioaerosols (Cariñanos et al., 2021; Rojo et al., 2015). For this study, a Doppler lidar system was operated at an olive orchard and at a peatland as important environments concerning their role for climate and human activities.

2. Experimental sites and instrumentation

The first rural location (Fig. 1) was an irrigated olive orchard in Úbeda, Spain (37.91°N, 3.23°W, 370 m a.s.l.). The site presents Mediterranean climate, with mean annual temperature of 16 °C and mean annual precipitation of 495 mm. Predominant surface winds come from NW during day and from S and SE at night (Aguirre-García et al., 2021; Chamizo et al., 2017). The site is located in a valley area, surrounded by Sierra Mágina and Sierra de Cazorla mountain ranges of >2100 m a.s.l., around 25 km at the Southwest and 45 km at the East, respectively. This kind of crop is one of the most important in the Mediterranean basin, particularly in Southern Spain. Therefore, its study and characterization are important in order to account for its impact on the global soil carbon cycle linked to anthropogenic climate change (Aguilera et al., 2015; Álvaro-Fuentes and Paustian, 2011; Vicente-Vicente et al., 2016). In

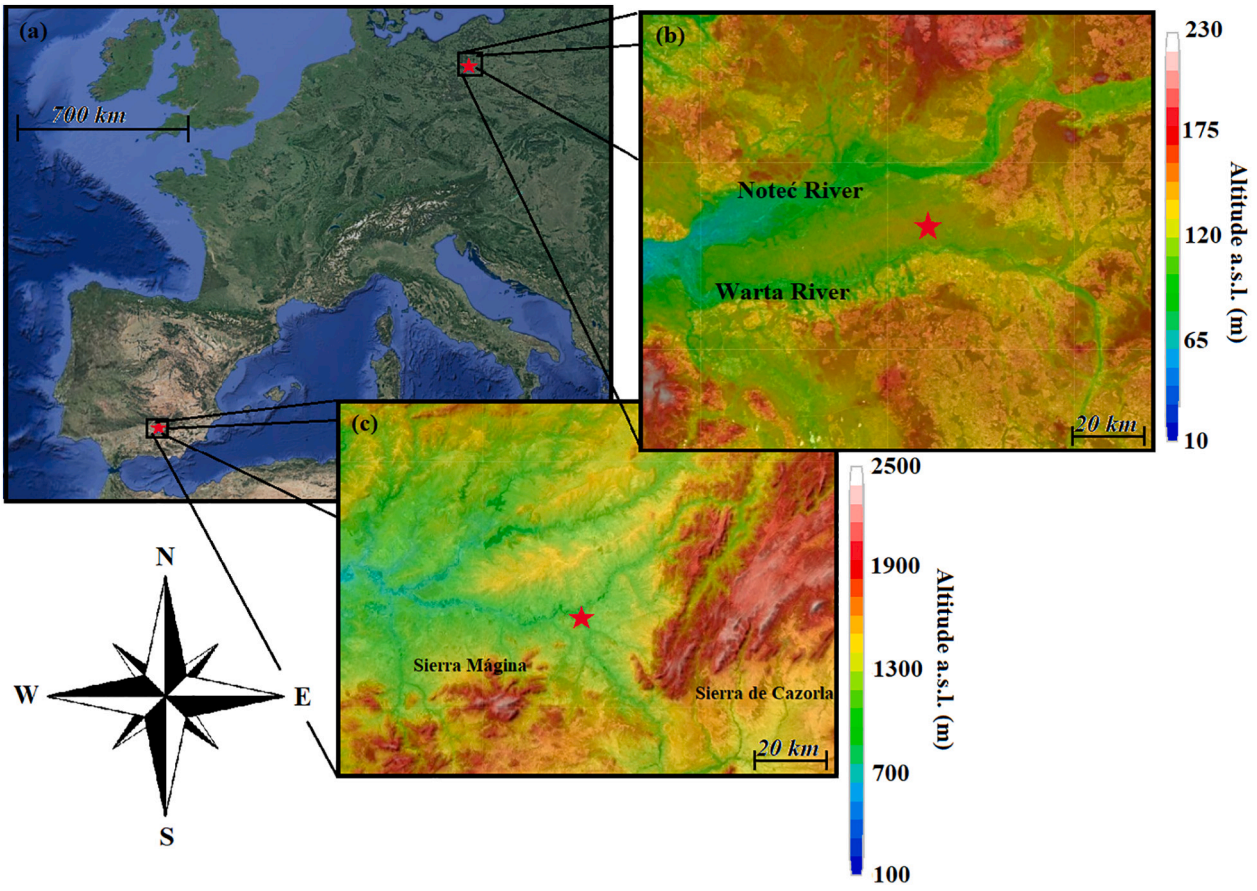

Fig. 1. Topographic maps showing with red stars the location of (a) Úbeda and Rzecin in Europe, (b) the peatland measurement station and (c) the olive orchard measurement station with respect to the surrounding orography. Images from earth.google.com and topographic-map.com (last access 5th July 2022). (For interpretation of the references to colour in this figure legend, the reader is referred to the web version of this article.)

particular, high turbulence conditions in the ABL over this kind of environments can cause important CO_2 ventilation episodes, which strongly determine and constrain other carbon cycle measurements and modelling (Moya et al., 2022). More information on the site description can be found in Chamizo et al. (2017) and Aguirre-García et al. (2021). The measurements campaigns AMAPOLA (Atmospheric Monitoring of Aerosol Particle Fluxes in Olive Orchard) and ABUNDANCE$_O$ (Rural Boundary Layer in Managed Ecosystems – Olive Orchard) were performed at this site. AMAPOLA and ABUNDANCE$_O$ campaigns were coordinated by the Atmospheric Physics Group (GFAT) of the University of Granada and funded in the framework of ACTRIS-2 and ELEMENTAL (Enabling Adaptation to Climate Change by Management of Ecosystem Carbon and Water Balance) projects, respectively. AMAPOLA was carried out from 18th to 29th April 2016, with the main focus of testing the combination of in-situ and remote sensing observations of aerosol particle fluxes. On the other hand, ABUNDANCE$_O$ was performed from 26th February to 26th March 2019 with the purpose of analysing the turbulent atmospheric structures and their impact on the closure energy balance at surface.

The second location (Fig. 1) was 'PolWet' site in Rzecin, Poland (52.75°N, 16.30°E, 59 m a.s.l.) of the Poznan University of Life Sciences (PULS), a peatland with average air temperature of 8.5 °C, annual precipitation of 526 mm and prevailing surface wind from W (Chojnicki et al., 2007; Harenda et al., 2021). The peatland rose as a result of lake shallowing (Barabach, 2013) and surrounded by Noteć Forest (Kondracki, 1998), is the place of measurements of CO_2/H_2O exchange between ecosystem and the atmosphere using the eddy covariance technique (Chojnicki et al., 2007) as well as conducted manipulation experiments (Górecki et al., 2021; Rastogi et al., 2019). Peatlands are a special type of wetland, representing one of the largest natural terrestrial carbon storages that have a strong interaction in the climate system (Harenda et al., 2018; Lappalainen, 1996). The measurement campaign POLIMOS-2018 (Polish Radar and Lidar Mobile Observation System) was performed at this site from 24th May to 24th September 2018 with the goal of assessing the impact of atmospheric optical properties on terrestrial ecosystem functioning. It was coordinated by the University of Warsaw (IGFUW) and funded by the European Space Agency.

The vertical profiles of 3D wind and of ABL turbulent properties were obtained in this study using the measurements of the Doppler lidar Stream Line (Halo Photonics), that is part of ACTRIS-Cloudnet (Illingworth et al., 2007). The system consists of a solid-state pulsed laser emitting at 1.5 μm and a heterodyne detector using fiber-optic technology. The emission is done with low pulse energy (100 μJ) and high pulse repetition rate (15 kHz). The signal acquisition is performed continuous and autonomously in vertical stare mode with a temporal resolution around 2 s, and it also has full hemispheric scanning capability. A more detailed description of this instrument can be found in (Ortiz-Amezcua et al., 2022).

3. Methodology

Doppler lidar instrument was configured to continuously perform vertically pointing measurements with a temporal resolution of 2 s, regularly interrupted to perform individual conical scans (Vertical-Azimuth-Display, VAD scans) with 12 equidistant azimuth points and constant elevation of 75° for AMAPOLA and 70° for ABUNDANCEo and POLIMOS. The scans were carried out every 10 min, 15 min and 30 min in each campaign, respectively. The instrument operated with the same range resolution of 30 m and an effective range from 90 m to 6000–9000 m.

In this study, we performed a statistical characterization of the field campaigns and the description of some particular cases. For such analysis, we used the products obtained with a standard software processing chain developed at the Finnish Meteorological Institute, called 'Halo lidar toolbox' (Manninen, 2019b).

Doppler lidar raw data processed by the toolbox are first corrected from the artefacts described by Manninen et al. (2016) and Vakkari et al. (2019), and the attenuated backscatter (β_{att}) is calculated from vertically pointing measurements signal intensity with the original time resolution and with the focus function as described by Pentikäinen et al. (2020). For our system, we used the experimentally obtained focal length of 535 ± 35 m and effective beam diameter of 17.5 ± 1.0 mm. From scanning measurements performed every 10, 15 min or 30 min (depending on the campaign), the 3D wind vector profiles are obtained with the Vertical-Azimuth-Display (VAD) method described by Newsom et al. (2017) and Päschke et al. (2015). From these wind profiles, wind shear (*sh*) vector is also calculated from the changes in the horizontal wind components (u and v) with height (e.g. ICAO, 2005), as it can be a source of turbulent mixing. For turbulence retrievals, the vertical velocity variance and skewness are calculated for each range gate from distributions corresponding to vertically pointing velocity measurements within 60-min time windows, using a method presented by Rimoldini (2014), which avoid biases from Gaussian noise and sample size. In particular, the vertical velocity skewness (S_w, obtained from the 3rd moment of the vertical velocity distribution, $\overline{(w-\overline{w})^3}$) is used in this study as an indicator of the predominant direction of the turbulent transport of turbulent kinetic energy (TKE), because $\overline{(w-\overline{w})^3}$ represents the vertical transport of variance (directly affecting TKE) by the turbulence itself. Therefore, positive S_w indicates that TKE is being transported upwards (and negative S_w downwards). The dissipation rate of the turbulent kinetic energy, ε, is calculated from the 3D wind vector profiles and the vertical velocity variance profiles, both previously interpolated to a common 3-min resolution. The method presented by O'Connor et al. (2010) is applied to obtain ε, which is used in this study as an indicator of turbulent mixing. According to this method, ε is calculated at each range gate from the vertical velocity variance (V_w) as:

$$\varepsilon = 2\pi\left(\frac{2}{3a}\right)^{3/2} \mathrm{V}_w{}^{3/2}\left(L^{2/3} - L_1{}^{2/3}\right)^{-3/2} \quad (1)$$

L_1 stands for the length scale corresponding to the eddies sampled by the lidar during 1 measurement and is estimated as the mean horizontal velocity times the lidar sampling time (2 s in this case), while L relates to the length scales of the largest eddies which pass completely through the lidar beam during the averaging window and $a = 0.55$ is the Kolmogorov constant for 1-dimensional wind spectra (Paquin and Pond, 1971).

Finally, all the calculated quantities are combined to create a bitfield-based classification mask described in Manninen et al. (2018), where further details on the software chain and the classification mask are given. This algorithm has the aim of objectively assigning a dominant source for turbulent mixing. After selecting regions with suitable signal for further analysis, this algorithm first creates a mask identifying the presence of turbulent mixing and whether it is associated with clouds, the surface, or neither. The cloud base height is first obtained and then a top-down approach is used to find all consecutive range gates below the cloud with turbulence presence and containing negative vertical velocity skewness. Similarly, surface-connected is resolved with a bottom-up approach until the first range gate where no turbulence is found. Turbulence identification is derived from ε with a threshold $\varepsilon > 10^{-5}$ m^2 s^{-3} or $\varepsilon > 10^{-4}$ m^2 s^{-3}, depending whether the classified heights were below cloud or connected to the surface (Manninen et al., 2018). Then, all range gates with surface-connected turbulent behaviour during daytime are classified as dominated by convective mixing. During night-time, when ABL is assumed to be neutral or stably stratified, wind-shear derived turbulence is searched with a threshold sh > 0.03 s^{-1} (Manninen, 2019a). Finally, range gates that are classified as turbulent but are unconnected to surface or clouds during daytime, and not related to wind shear during night-time, are labelled as 'intermittent' since turbulence is assumed to arise from other intermittent sources (Lothon et al., 2014).

After the application of the processing chain to the databases, an

additional criterion was used to ensure statistical representativity for the statistical analysis. Wind retrieval was not available for certain time and altitude gates where the signal-to-noise ratio was not enough (using a threshold of −22.2 dB), when the quality of the retrieval was not enough (using R^2 threshold of 0.95), where precipitation or fog was detected or if there were no measurements (because of technical issues). With this in mind, the fraction of the data from the total analyzed period that were available was calculated for each hour of the day and altitude gate, and we selected the ones with >60% availability to perform the statistical analysis.

4. Results

4.1. Horizontal wind statistical characterization

Fig. 2 shows the time evolution of the hourly averaged wind speed (U_H) profiles, from 100 m a.g.l. to the maximum available altitude gate (following the 60% availability criterion), over all measurements taken each hour during the campaigns. Subplots (a), (c) and (e) include the number of profiles that were averaged for each of the resulting profiles in subplots (b), (d) and (f), respectively. From subplots (b) and (d), a quite similar behaviour can be observed for AMAPOLA and ABUNDANCEo campaigns, although the first one present less smooth average profiles because of the shorter averaged period (12 days). This similar diurnal evolution is, therefore, interpreted as typical for this location at that time of the year (March–April). For this site, three different time intervals can be identified in terms of average wind profiles: evening and night (from around 16–17 h UTC to 7–8 h UTC) with moderate winds around 5 m/s showing a height profile with a maximum around 500 m a.g.l. that reaches up to 10 m/s at 19 h UTC for ABUNDANCEo and at 17 h UTC for AMAPOLA; low winds in the morning (from around 7–8 h UTC to 11–12 h UTC) with speeds increasing with height up to 5 m/s, and constant wind profiles at noon and afternoon (11–12 h UTC to 16–17 h UTC).

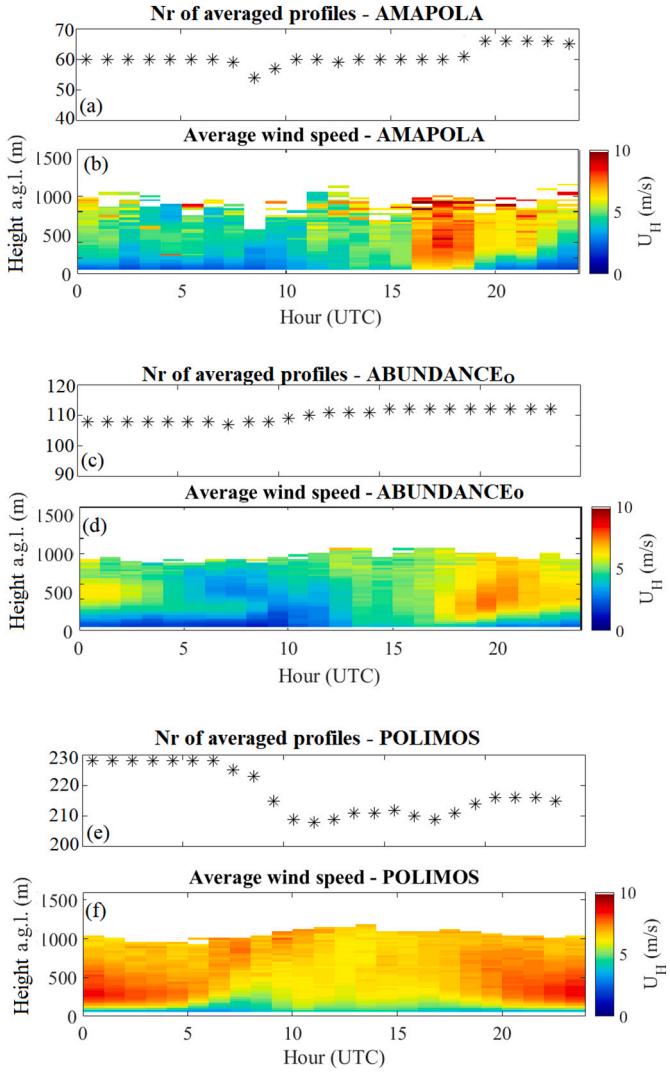

Fig. 2. Hourly averages of horizontal wind speed vertical profiles for the three campaigns.

Results for the polish site (Fig. 2c) during POLIMOS revealed some similarities and also some differences with respect to the location in South Spain. Firstly, the average wind speeds were higher than in the olive orchard campaigns during the whole day and for all heights. Moreover, the diurnal pattern seemed to be strongly influenced by the ABL development during daytime. The nighttime winds were strong for this site, with averages close to 10 m/s for all heights, although the height profiles also presented maximum speeds around 400–500 m a.g.l. The daytime winds increased with height, with lowest velocities in the central hours of the day.

In order to characterize wind directions, a wind rose study was performed for the analyzed campaigns. We divided the hourly averaged profiles into three height regions, namely 100–340 m a.g.l., 340–580 m a.g.l. and 580–820 m a.g.l. Higher altitudes were not considered since they did not fulfilled the 60% availability criterion. We also distinguished between two time intervals: 'Daytime' and 'Nighttime', which were defined for each campaign as the hours when it was daytime (or nighttime) for all the included days (considering the seasonal insolation changes). The daytime hours were 05:30–18:50 h, 06:50–18:00 h and 04:45–16:45 h UTC for AMAPOLA, ABUNDANCEo and POLIMOS, respectively, and the nighttime hours were 20:40–03:40 h, 20:00–04:40 and 21:40–00:15 h UTC, respectively. With this height and time intervals, a total of six different wind roses for each campaign are depicted in.

Fig. 3 with 45° angle intervals and the wind speed intervals: 0.0–2.5 m/s, 2.5–5.0 m/s, 5.0–7.5 m/s, 7.5–10.0 m/s and ≥ 10.0 m/s.

The wind roses for both campaigns at the Iberian mountainous site presented similarities, as in the case of wind speed averages, indicating a general behaviour of the atmosphere over that location for those months. In general terms, the predominant wind directions for both sites were W and NW, what is to be expected due to the most frequent synoptic patterns in the northern hemisphere. However, the winds over the olive orchard presented more marked modes of variation. A strong contribution from S and SE was present in nighttime winds below 340 m a.g.l. during ABUNDANCEo and AMAPOLA, with greater speeds in the latter campaign. These southern winds lost importance at greater heights, with almost no presence in AMAPOLA. This pattern is consistent with mountain-valley flows due to the close presence of mountains at the SW and E of the measuring site. During ABUNDANCEo, moreover, a non-negligible SE contribution was present at those lowest heights also during daytime.

The wind roses corresponding to POLIMOS reveal that the western winds were predominant during daytime at all heights, with greater speeds than in the mountainous site. During nighttime, the distribution of the winds was almost homogeneous, with high frequency of winds of >10 m/s, especially for the central height range.

4.2. Frequency and effect of clouds during the campaigns. Turbulence case studies

The presence of ABL clouds can significantly influence the behaviour and development of the ABL. When they cover the ABL, they reduce the solar radiation reaching the surface, which directly decreases the available energy of convective mixing. Moreover, cloud-top radiative cooling can be dominant driver for turbulent mixing in an inverse

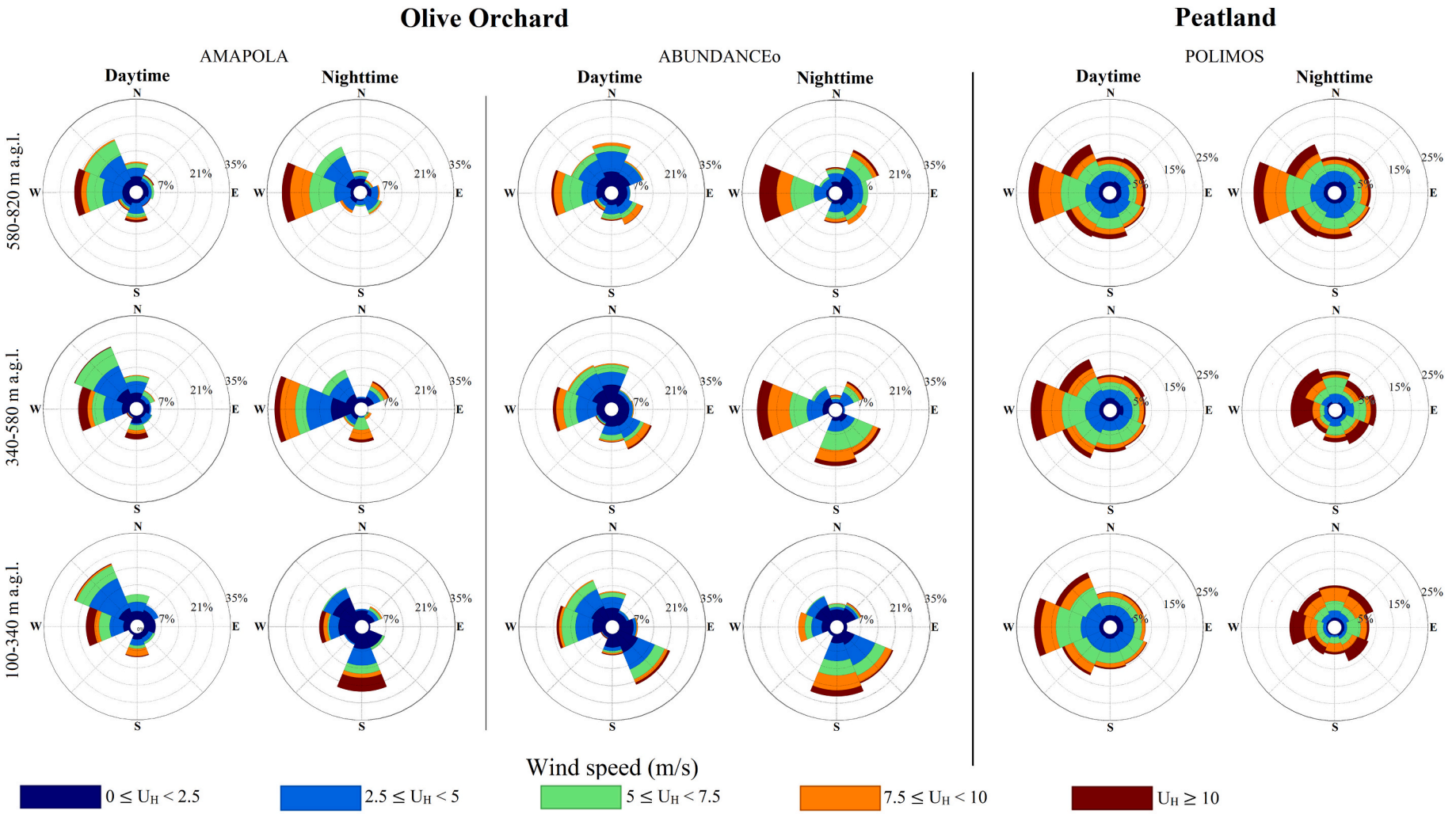

Fig. 3. Wind roses showing the prevailing wind speeds and directions during the campaigns within three different height ranges: 100–340 m (lower row), 340–580 m (central row) and 580–820 m a.g.l. (upper row). For each campaign, daytime hours (left columns) and nighttime hours (right cloumns) are also distinguished.

process of the surface-driven turbulence, i.e., by favouring negatively buoyant plumes generated at cloud top (Hogan et al., 2009; Wood, 2012). Therefore, it is important to consider the presence of clouds within and on the ABL top during the analyzed periods to properly interpret further results. In Fig. 4, the frequency of detected clouds is depicted for all times. Note that, due to the different temporal scope of the campaigns, these results must be differently interpreted. The cloud presence during AMAPOLA (Fig. 4a) was quite frequent at all heights over around 1 km a.g.l., a result that provides information on the particular meteorological conditions during that period. For ABUNDANCEo, Fig. 4b shows a band of clouds between 1 and 3 km in the morning, which around 9–10 h starts to rise and increase its frequency following a shape similar to the typical ABL height diurnal cycle. The cloud band seems to be above the ABL with a vertical extension of roughly 2 km. For POLIMOS (Fig. 4c), however, the plot shows a more important presence of clouds from 10 to 16 h UTC, with altitudes rising from 1 km to around 3 km a.g.l. with time. The longer duration of POLIMOS campaign makes this result more representative of the Polish flat-terrain peatland in summer 2018, and this effect can be considered a more general behaviour likely also linked to the ABL convective growth.

In the view of the non-negligible presence of clouds during the three studied campaigns, with frequencies reaching up to 30% for some heights and times, the case studies shown are focused on the effects commonly observed at both locations under cloud-topped boundary layer (CTBL) versus non-CTBL conditions. Only one case is represented for each type of conditions, because the observed effects of clouds were found to be similar in both sites during the three campaigns.

Fig. 5 shows the temporal evolution of attenuated backscatter (β_{att}), TKE dissipation rate (ε), vertical wind skewness (S_w), horizontal wind speed (U_H) and direction, wind shear (sh) and ABL classification mask obtained from the Halo toolbox processing chain for 28 April 2016 during AMAPOLA campaign, as an example when the ABL was not topped by clouds. This can be verified in Fig. 5a, where the whole ABL (below around 2 km a.g.l.) remained with β_{att} values below the cloud threshold. The temporal evolution of ε (Fig. 5b) indicates that turbulence started in the very low layers around sunrise (at 05:26 h UTC) and created a turbulent layer that grew until reaching about 2 km a.g.l. at noon. This turbulent growing layer presented strongly positive skewness

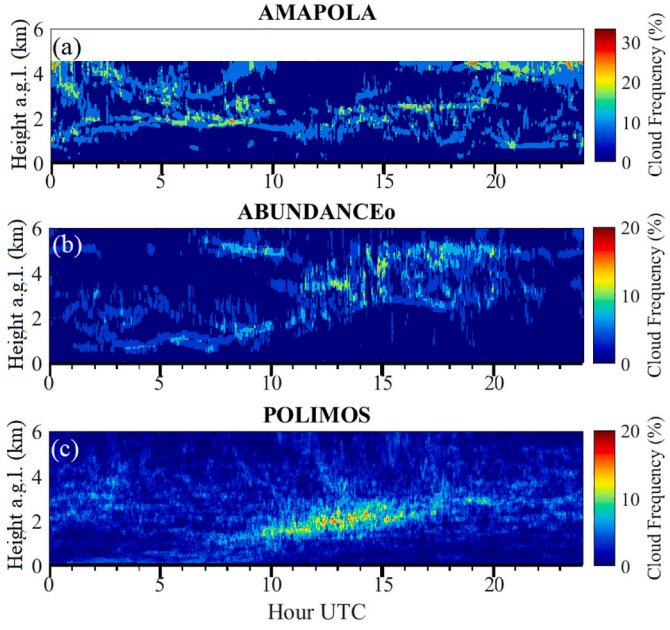

Fig. 4. Frequency of occurrence of clouds with height and time resolution for the three campaigns. Note that colour scales are different to improve clarity of the plots.

(Fig. 5c), and therefore could be classified as convective mixing (Fig. 5g). In coincidence with the increasing turbulence, it is noticeable the decrease of β_{att} (Fig. 5a), meaning that in absence of strong sources, aerosol concentration reduced as particles were mixed in a higher column. The convection was dominant during the whole day, allowing the development of the ABL until sunset (at 18:56 h UTC that day). After that, ε strongly decreased and aerosol was more concentrated again, with increasing β_{att}. This sudden stop of convection was well captured by the classification mask (Fig. 5g), although some remaining turbulence was still detected at different heights after sunset. That turbulence was labelled as intermittent by the classification mask, since it was unconnected with surface or with any strong wind shear (Lothon et al., 2014; Manninen et al., 2018).

This example case also illustrates the wind-shear driven turbulence. Wind shear vector (Fig. 5f) displayed strong variations from 0 up to 0.06 s^{-1} inside the convective growing layer, but the algorithm always assumes that convective mixing dominates as turbulence source when present. However, in the hours before sunrise, the presence of a low-level jet (Blackadar, 1957), shown by the higher wind speeds between 500 and 1000 m a.g.l. (Fig. 5d) together with a different direction with respect to lower and higher altitudes (Fig. 5e), created two layers with wind shear values larger than 0.02 s^{-1} (Fig. 5f). Those layers produced nocturnal turbulence in a stratified pattern, with high ε values close to the surface and in the elevated layer around 1 km a.g.l. This pattern coincided with negative S_w values (blue areas before 5 h UTC in Fig. 5c), with a layer of positive S_w in between. The BL-classification mask (Fig. 5g) labelled those altitude gates as turbulent, with source in wind shear.

The second analyzed case corresponds to 14 September 2018, at the Polish location during POLIMOS. In this case, some low clouds were present, interacting with the ABL turbulence evolution. Fig. 6 shows the temporal evolution of the same relevant variables as in previous case. High β_{att} values (red colour in Fig. 6a) revealed the cloud presence during almost the whole day, most of the time at the top of the detected ABL (around 1 km a.g.l.). During the early morning, around 6 h UTC, some very low clouds were formed at <0.5 km a.g.l., coinciding with the starting of the convective turbulence as evidenced by growing ε values (Fig. 6b) and positive S_w (Fig. 6c) and correctly labelled by the classification mask (Fig. 6g).

The effect of the clouds observed at 1 km a.g.l. during nighttime (00:00 to 05:30 h UTC) was the predominance of downdrafts, revealed by the negative S_w below that height (Fig. 6c). These downdrafts produced slightly higher values of ε in a more or less homogeneous layer of 200 m below the clouds (Fig. 6b), being thus classified as cloud-driven turbulence (Fig. 6g). That classification, however, might not to be providing correct label before around 02:00 h UTC, when turbulence over 500 m a.g.l. was interpreted as 'intermittent'. This may probably be caused by the apparent lack of connection between that area and the clouds above, actually due to the lack of enough signal.

On the other hand, the effect of the clouds that were present on top of the convective layer, at 1.5 km a.g.l. around 13:30 h UTC seemed to avoid the further growth of that layer, that sharply stopped the upwards movements (positive S_w) and decreased its ε values although sunset was later around 17 h UTC that day. After this effect, some turbulence was detected at layers unconnected from the surface from around 0.5 km up to >1 km a.g.l., what could be related to the dissipation of the turbulent energy from the disappearing convective layer. Horizontal winds for that day (Fig. 6 d, e) were low and only created some layers with moderate wind shear (Fig. 6 f), not able to significantly produce associated turbulence. The classification mask (Fig. 6 g), therefore, labelled those moderately turbulent layers after sunset as presenting 'intermittent' turbulence.

4.3. Statistical characterization of turbulence sources

The ABL-classification mask from 'Halo lidar toolbox' was applied to

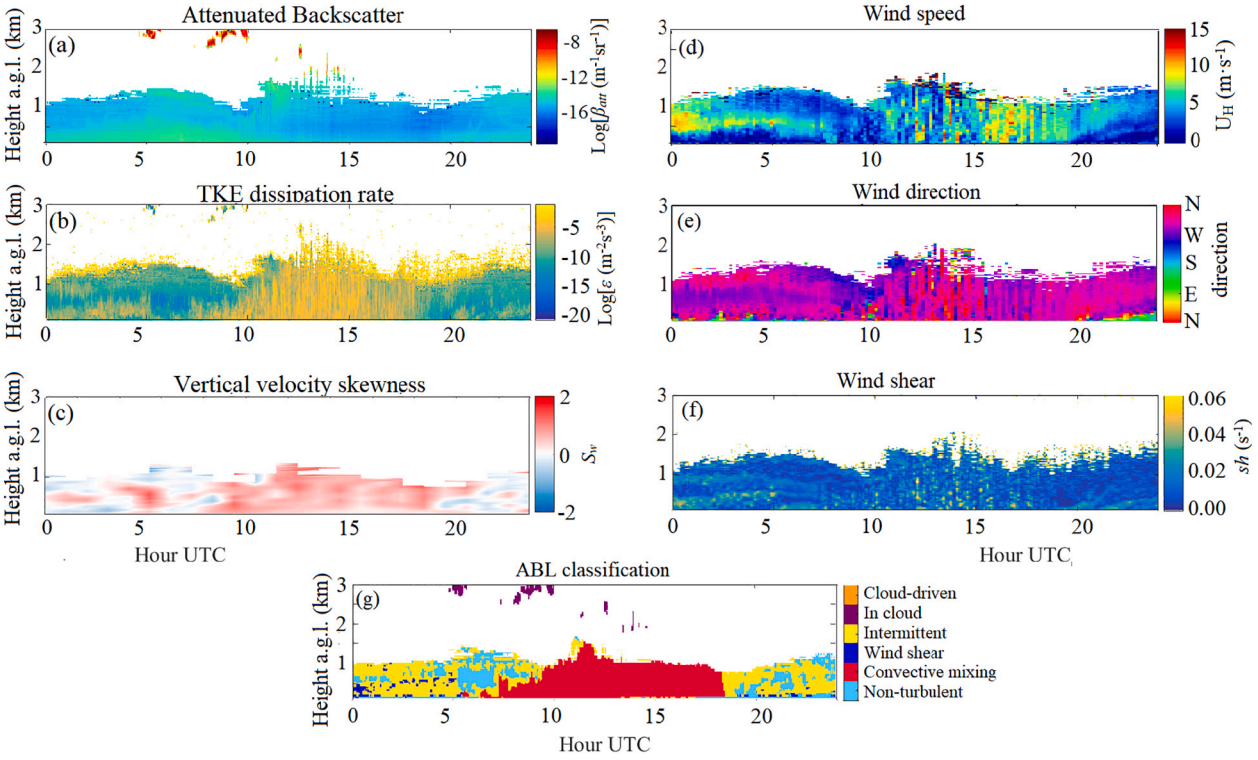

Fig. 5. Time evolution of the vertical profiles of (a) attenuated backscatter, (b) TKE dissipation rate, (c) vertical velocity skewness, (d) horizontal wind speed, (e) horizontal wind direction, (f) wind shear, and (g) ABL classification mask, calculated for a non-CTBL case measured on 28 April 2016 during AMAPOLA.

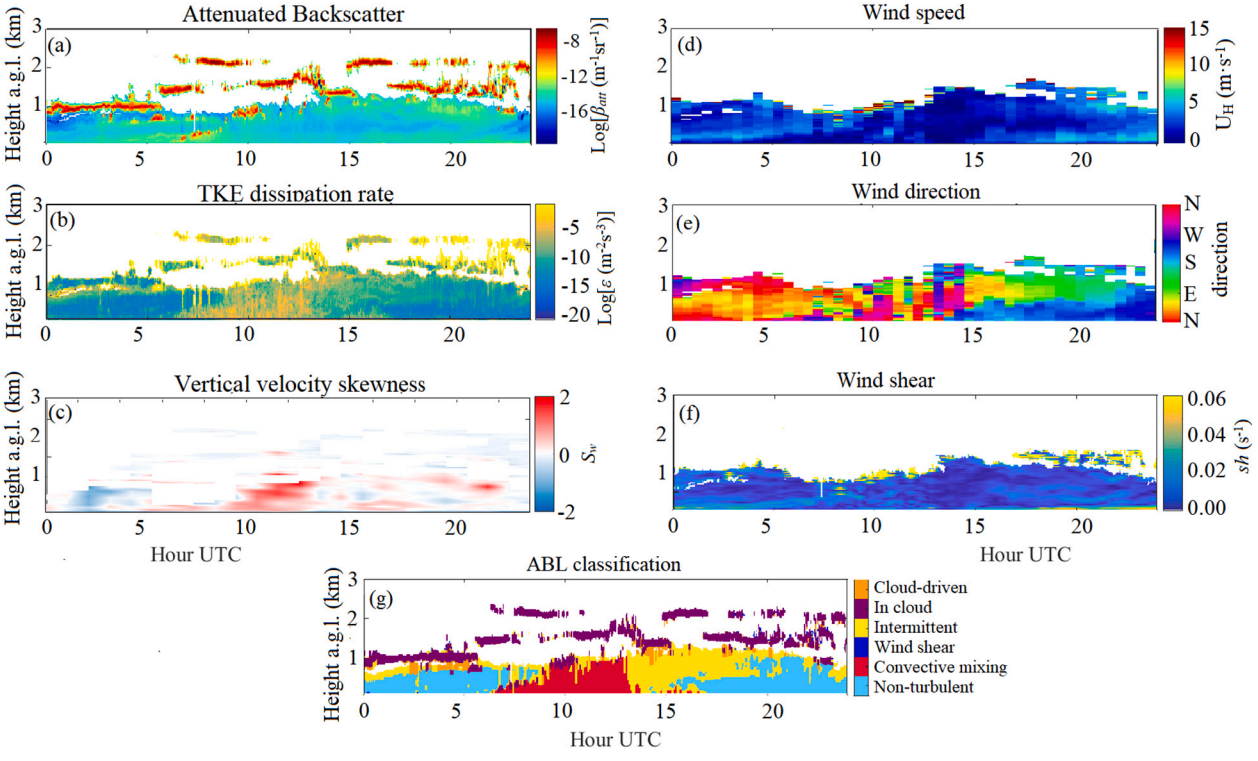

Fig. 6. Time evolution of the vertical profiles of (a) attenuated backscatter, (b) TKE dissipation rate, (c) vertical velocity skewness, (d) horizontal wind speed, (e) horizontal wind direction, (f) wind shear, and (g) ABL classification mask, calculated for a cloudy case measured on 14 September 2018 during POLIMOS.

the three campaigns. Then, the frequency of each turbulent source was calculated with time and height resolution, in order to identify the general behaviour of the analyzed campaigns in terms of turbulence. It is important to notice that in the view of the previous cases, the resulting frequencies could be slightly underestimated, especially at heights close to the top of the ABL. The lack of enough quality signal, sometimes

occurring at those heights, might lead to a wrong application of the first mask, classifying the turbulence as unconnected from surface or from clouds when there are intermediate pixels that were filtered out. Fig. 7 displays the results for the three main turbulence sources, namely 'convective' (Fig. 7a, d, g), 'wind shear driven' (Fig. 7b, e, h) and cloud driven (Fig. 7c, f, i). Although a very similar behaviour could be found in terms of horizontal wind in Subsection 4.1 for the two campaigns at the Spanish site, the results were not very similar in terms of turbulence sources. Therefore, the different month of the year and the particular cloud and meteorological conditions of the campaigns played a major role in the turbulent behaviour.

The convective mixing frequency plots show a clear diurnal evolution for the two sites, as it was already illustrated with the study cases in the previous subsection. This mechanism usually starts with sunrise in the lowest heights and is more frequent at growing altitudes up to a maximum. For POLIMOS and ABUNDANCEo, this maximum height was around 600 m a.g.l. for ~70% of the measurements in the central hours of the day, and reached almost 1000 m a.g.l. in ~40% of the cases. The conditions during AMAPOLA, however, decreased that maximum height down to around 400 m a.g.l. in 60% of cases, reaching >500 m a.g.l. in <30% of cases.

Wind shear plots only present frequency values during nighttime, since convective mixing is assumed to dominate the surface-connected turbulence when it is present (during daytime). ABUNDANCEo was the campaign with more detected wind shear driven turbulence, with frequencies around 20% in all heights from the surface up to 600 m a.g.l. During AMAPOLA, the turbulence due to this mechanism was very superficial in the evening and located in a decoupled layer around 300 m a.g.l. from 00 to 05 h UTC. Wind shear driven turbulence was also relevant in the peatland site, but it was always detected below 100 m a.g.l. Despite the different height distributions of wind shear, we observed frequencies larger than 40% for some ranges and times at both rural sites, making this mechanism much more relevant than in urban environment as observed e.g. in Granada city (Ortiz-Amezcua et al., 2022).

Finally, the cloud driven turbulence frequency was also represented, although the frequency of this mechanism was much lower than the rest (<10% frequency). Moreover, the frequency of this mechanism is completely influenced by the particular conditions during AMAPOLA and even during ABUNDANCEo, due to their more limited duration. For POLIMOS, however, we conclude that clouds were able to produce turbulence mainly during the central hours of the day at heights between 600 and 1000 m a.g.l., with frequencies around 5%.

5. Conclusions and final remarks

Two different rural sites were characterized in terms of horizontal wind field and turbulence by Doppler lidar technique. The statistical analysis of the horizontal wind for the three analyzed campaigns indicated a general trend of winds blowing from W with the highest speeds during nighttime, a feature that was not found in other studies. Higher

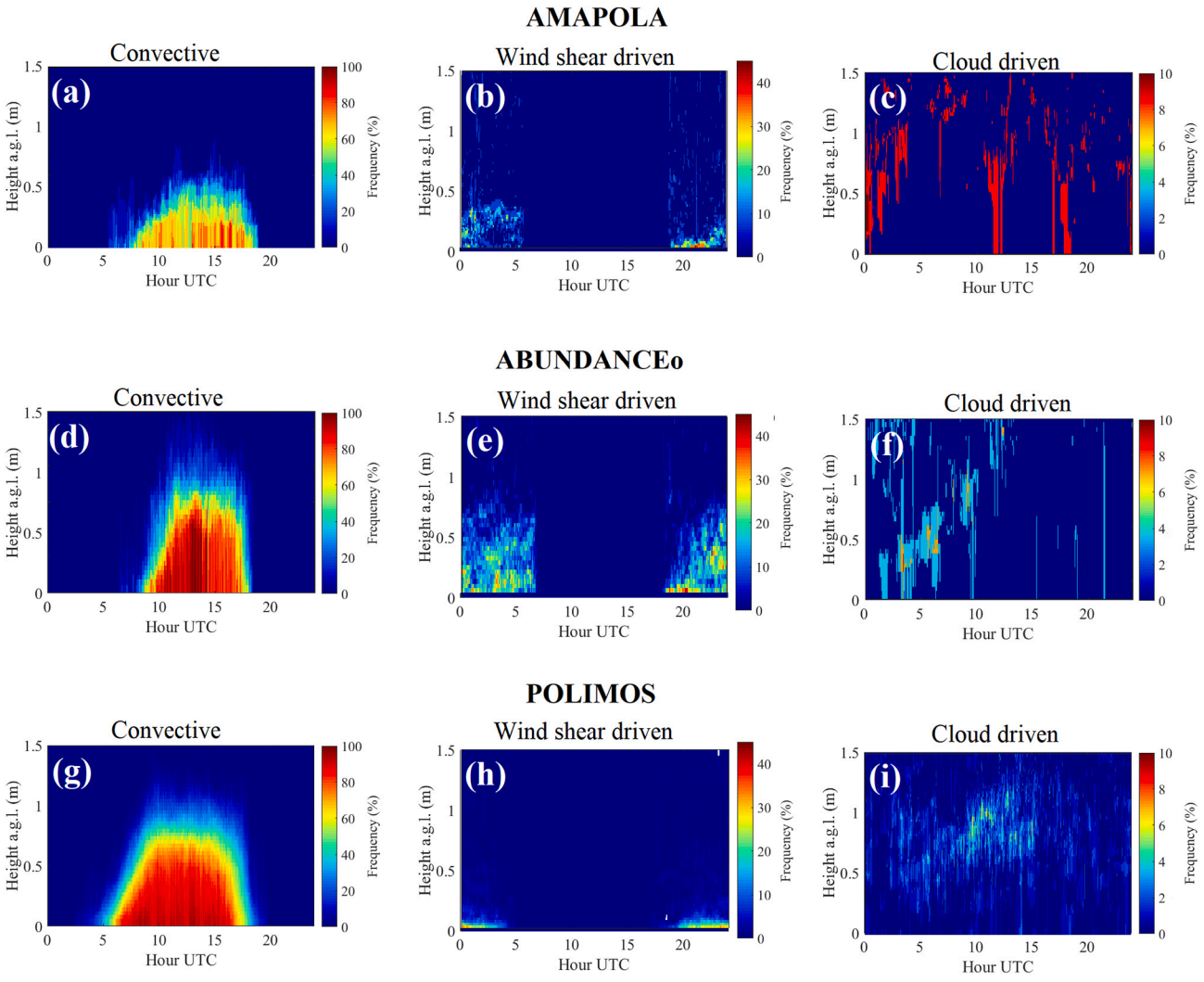

Fig. 7. Frequency of occurrence of the three main turbulence sources for each time and altitude gates, and for each campaign.

average speeds were found for the flat-terrain peatland site, where the diurnal evolution showed a clear pattern dominated by the daytime ABL growth. For the mountainous olive orchard in South Spain, an important contribution of winds from S was found during nighttime, in consonance with the flows generated by the surrounding mountains. From this analysis, the strong capability of Doppler lidar to provide enough valuable data to perform robust statistical analysis was demonstrated, with the added value of the vertical resolution apart from the high temporal resolution. This allowed for separating different wind contributions or patterns, in terms of speed and direction, at the different heights in the analyzed locations, crucial information for a correct modelling of such environments.

The turbulence analysis appeared to be more dependent on the particular meteorological conditions during the measurement campaign, with a strong influence of boundary layer clouds presence. The non-CTBL case showed a typical situation where ABL is fully developed during daytime due to convection, with high turbulent activity (in terms of ε) and strong positive skewness indicating frequent and powerful updrafts. The cloud-topped case showed the strong influence that clouds can have on ABL developement, avoiding it to reach the same maximum height and introducing top-down movements as important contribution to mixing. The statistical analysis of turbulent sources showed a similar importance and height distribution of daytime convective mixing at both locations, excepting for the cloud influence during AMAPOLA campaign. Wind shear mechanism was found to be present also with similar frequencies, but homogenously distributed up to 600 m a.g.l. for the olive orchard and concentrated below 100 m a.g.l. for the peatland site. Cloud driven turbulence was found to be a non-negligible contribution during the studied campaigns.

The analysis of example cases and the statistical analysis illustrated the strong capabilities of the applied algorithms, and also some of its limitations. The classification mask was able to identify even quick changes in the turbulence regime, for example due to the stop or decrease of the incoming solar radiation due to sunset or the presence of boundary layer clouds, due to the presence of strong shears, or negatively buoyant plumes from boundary layer clouds. However, one of the limitations was the attribution of turbulence to a single dominant source, without the possibility of quantifying the presence of simultaneous sources. It is suggested, and likely possible to achieve with Doppler lidar measurements, to include a new mask providing a level of confidence or probability to the different identified sources in future versions of the algorithm. Moreover, the classification of turbulence as surface-connected, cloud-connected, or unconnected should take into account the possibility that some pixels are not available due to filtering so that the connection with the mentioned sources is not artificially lost. Those recommendations would enhance the robustness of the algorithm and improve the general understanding of further explored databases similar to the ones presented here.

CRediT authorship contribution statement

Pablo Ortiz-Amezcua: Conceptualization, Data curation, Formal analysis, Investigation, Writing – original draft, Writing – review & editing. **Juana Andújar-Maqueda:** Data curation, Formal analysis, Writing – review & editing. **Antti J. Manninen:** Methodology, Software, Writing – review & editing. **Pyry Pentikäinen:** Methodology, Software, Writing – review & editing. **Ewan J. O'Connor:** Methodology, Software, Writing – review & editing. **Iwona S. Stachlewska:** Funding acquisition, Investigation, Project administration, Writing – review & editing. **Gregori de Arruda Moreira:** Data curation, Writing – review & editing. **José Antonio Benavent-Oltra:** Investigation, Writing – review & editing. **Juan Andrés Casquero-Vera:** Investigation, Writing – review & editing. **Patryk Poczta:** Investigation, Writing – review & editing. **Dongxiang Wang:** Investigation, Writing – review & editing. **Kamila M. Harenda:** Investigation, Writing – review & editing. **Bogdan H. Chojnicki:** Funding acquisition, Project administration, Writing – review & editing. **Dominika M. Szczepanik:** Writing – review & editing. **Łucja Janicka:** Writing – review & editing. **Dirk Schüttemeyer:** Funding acquisition, Project administration, Writing – review & editing. **Lucas Alados-Arboledas:** Conceptualization, Funding acquisition, Project administration, Writing – review & editing. **Juan Luis Guerrero-Rascado:** Conceptualization, Funding acquisition, Project administration, Writing – review & editing.

Declaration of Competing Interest

The authors declare that they have no known competing financial interests or personal relationships that could have appeared to influence the work reported in this paper.

Data availability

Data will be made available on request.

Acknowledgement

This research has been done primarily thanks to the financial support of Fundación Ramón Areces through grant 'Ampliación de estudios en el extranjero en Ciencias de la Vida y de la Materia. XXXII Convocatoria'.

An important part of the work has also been performed in the frame of the Technical assistance for Polish Radar and Lidar Mobile Observation System (POLIMOS) funded by ESA-ESTEC Contract no. 4000119961/16/NL/FF/mg and is also partially supported by Polish National Science Centre (NCN) through project 2021/40/C/ST10/00023 of programme SONATINA 5.

This work was also supported by the Spanish Ministry of Economy and Competitiveness through projects CGL2015-73250-JIN, CGL2016-81092-R, CGL2017-83538-C3-1-R, CGL2017-90884-REDT, PID2020-117825GB-C21 and PID2020-120015RB-100. The Andalusian Regional Government has funded this work through project P18-RT-3820.. The authors thankfully acknowledge the FEDER-UGR program (reference A-RNM-430-UGR20) for the instrumentation used in this work and the University of Granada that supported this study through the Excellence Units Program. ACTRIS-2 Research Infrastructure Project of the European Union's Horizon 2020 research and innovation program (grant agreement No 654109). This work contributes towards European Cooperation in Science and Technology (COST Action: PROBE, CA18235). Funding for open access charge: Universidad de Granada / CBUA.

References

Aguilera, E., Guzmán, G., Alonso, A., 2015. Greenhouse gas emissions from conventional and organic cropping systems in Spain. II. Fruit tree orchards. Agron. Sustain. Dev. 35 (2), 725–737. https://doi.org/10.1007/S13593-014-0265-Y.

Aguirre-García, S.D., Aranda-Barranco, S., Nieto, H., Serrano-Ortiz, P., Sánchez-Cañete, E.P., Guerrero-Rascado, J.L., 2021. Modelling actual evapotranspiration using a two source energy balance model with Sentinel imagery in herbaceous-free and herbaceous-cover Mediterranean olive orchards. Agric. For. Meteorol. 311, 108692 https://doi.org/10.1016/J.AGRFORMET.2021.108692.

Álvaro-Fuentes, J., Paustian, K., 2011. Potential soil carbon sequestration in a semiarid Mediterranean agroecosystem under climate change: quantifying management and climate effects. Plant Soil 338 (1). https://doi.org/10.1007/s11104-010-0304-7.

Barabach, J., 2013. The history of Lake Rzecin and its surroundings drawn on maps as a background to palaeoecological reconstruction. Limnol. Rev. 12 (3) https://doi.org/10.2478/v10194-011-0050-0.

Blackadar, A.K., 1957. Boundary layer wind maxima and their significance for the growth of nocturnal inversions. Bull. Am. Meteorol. Soc. 38 (5) https://doi.org/10.1175/1520-0477-38.5.283.

Bossioli, E., Tombrou, M., Dandou, A., Athanasopoulou, E., Varotsos, K.V., 2009. The role of planetary boundary-layer parameterizations in the air quality of an urban area with complex topography. Bound. Layer Meteorol. 131 (1), 53–72. https://doi.org/10.1007/s10546-009-9349-7.

Bowling, D.R., Massman, W.J., 2011. Persistent wind-induced enhancement of diffusive CO2 transport in a mountain forest snowpack. J. Geophys. Res. Biogeosci. 116 (4) https://doi.org/10.1029/2011JG001722.

Cariñanos, P., Foyo-Moreno, I., Alados, I., Guerrero-Rascado, J.L., Ruiz-Peñuela, S., Titos, G., Cazorla, A., Alados-Arboledas, L., Díaz de la Guardia, C., 2021. Bioaerosols

in urban environments: trends and interactions with pollutants and meteorological variables based on quasi-climatological series. J. Environ. Manag. 282, 111963 https://doi.org/10.1016/J.JENVMAN.2021.111963.
Chamizo, S., Serrano-Ortiz, P., López-Ballesteros, A., Sánchez-Cañete, E.P., Vicente-Vicente, J.L., Kowalski, A.S., 2017. Net ecosystem CO2 exchange in an irrigated olive orchard of SE Spain: influence of weed cover. Agric. Ecosyst. Environ. 239, 51–64. https://doi.org/10.1016/j.agee.2017.01.016.
Chojnicki, B.H., Urbaniak, M., Józefczyk, D., Augustin, J., Olejnik, J., 2007. Measurements of gas and heat fluxes at Rzecin wetland. In: Okruszko, T., Malby, E., Szatylowicz, J., Swiatek, D., Kotowski, W. (Eds.), Wetlands: Monitoring, Modeling and Management. Taylor & Francis, London, England, pp. 125–131.
Cimini, D., Haeffelin, M., Kotthaus, S., Löhnert, U., Martinet, P., O'Connor, E., Walden, C., Coen, M.C., Preissler, J., 2020. Towards the profiling of the atmospheric boundary layer at European scale—introducing the COST Action PROBE. Bull. Atmos. Sci. Technol. 1 (1), 23–42. https://doi.org/10.1007/s42865-020-00003-8.
Gökçek, M., Bayülken, A., Bekdemir, Ş., 2007. Investigation of wind characteristics and wind energy potential in Kirklareli, Turkey. Renew. Energy. https://doi.org/10.1016/j.renene.2006.11.017.
Górecki, K., Rastogi, A., Stróżecki, M., Gąbka, M., Lamentowicz, M., Łuców, D., Kayzer, D., Juszczak, R., 2021. Water table depth, experimental warming, and reduced precipitation impact on litter decomposition in a temperate Sphagnum-peatland. Sci. Total Environ. 771 https://doi.org/10.1016/j.scitotenv.2021.145452.
Harenda, K.M., Lamentowicz, M., Samson, M., Chojnicki, B.H., 2018. The role of peatlands and their carbon storage function in the context of climate change. In: GeoPlanet: Earth and Planetary Sciences.
Harenda, K.M., Samson, M., Juszczak, R., Markowicz, K.M., Stachlewska, I.S., Kleniewska, M., Macarthur, A., Schüttemeyer, D., Chojnicki, B.H., 2021. Impact of atmospheric optical properties on net ecosystem productivity of peatland in poland. Remote Sens. 13 (11) https://doi.org/10.3390/rs13112124.
Hogan, R.J., Grant, A.L.M., Illingworth, A.J., Pearson, G.N., O'Connor, E.J., 2009. Vertical velocity variance and skewness in clear and cloud-topped boundary layers as revealed by Doppler lidar. Q. J. R. Meteorol. Soc. 135, 635–643. https://doi.org/10.1002/qj.413.
ICAO, 2005. Manual on Low-level Wind Shear,. Doc 9817 AN/449.
Illingworth, A.J., Hogan, R.J., O'Connor, E.J., Bouniol, D., Brooks, M.E., Delanoë, J., Donovan, D.P., Eastment, J.D., Gaussiat, N., Goddard, J.W.F., Haeffelin, M., Klein Baltinik, H., Krasnov, O.A., Pelon, J., Piriou, J.M., Protat, A., Russchenberg, H.W.J., Seifert, A., Tompkins, A.M., van Zadelhoff, G.J., Vinit, F., Willen, U., Wilson, D.R., Wrench, C.L., 2007. Cloudnet: continuous evaluation of cloud profiles in seven operational models using ground-based observations. Bull. Am. Meteorol. Soc. https://doi.org/10.1175/BAMS-88-6-883.
Illingworth, A.J., Cimini, D., Gaffard, C., Haeffelin, M., Lehmann, V., Löhnert, U., O'Connor, E.J., Ruffieux, D., 2016. Exploiting existing ground-based remote sensing networks to improve high-resolution weather forecasts. Bull. Am. Meteorol. Soc. 96 (12), 2107–2125. https://doi.org/10.1175/BAMS-D-13-00283.1.
Kondracki, J., 1998. Polish Regional Geography. Warszawa, Wydawnictwo Naukowe PWN.
Kotthaus, S., Bravo-Aranda, J.A., Collaud Coen, M., Guerrero-Rascado, J.L., Costa, M.J., Cimini, D., O'Connor, E.J., Hervo, M., Alados-Arboledas, L., Jiménez-Portaz, M., Mona, L., Ruffieux, D., Illingworth, A., Haeffelin, M., 2022. Atmospheric boundary layer height from ground-based remote sensing: a review of capabilities and limitations. Atmos. Meas. Tech. Discuss. https://doi.org/10.5194/amt-2022-14 in review.
Lappalainen, E., 1996. General review on world peatland and peat resources. In: Lappalainen, E. (Ed.), Global Peat Resources. International Peat Society and Geological Survey of Finland, Jyska, Finland, pp. 53–55.
Li, J., Yu, X., 2017. LiDAR technology for wind energy potential assessment: DEMONSTRATION and validation at a site around Lake Erie. Energy Convers. Manag. 144, 252–261. https://doi.org/10.1016/j.enconman.2017.04.061.
Lothon, M., Lohou, F., Pino, D., Couvreux, F., Pardyjak, E.R., Reuder, J., Vilà-Guerau De Arellano, J., Durand, P., Hartogensis, O., Legain, D., Augustin, P., Gioli, B., Lenschow, D.H., Faloona, I., Yagüe, C., Alexander, D.C., Angevine, W.M., Bargain, E., Barrié, J., Bazile, E., Bezombes, Y., Blay-Carreras, E., Van De Boer, A., Boichard, J.L., Bourdon, A., Butet, A., Campistron, B., De Coster, O., Cuxart, J., Dabas, A., Darbieu, C., Deboudt, K., Delbarre, H., Derrien, S., Flament, P., Fourmentin, M., Garai, A., Gibert, F., Graf, A., Groebner, J., Guichard, F., Jiménez, M.A., Jonassen, M., Van Den Kroonenberg, A., Magliulo, V., Martin, S., Martinez, D., Mastrorillo, L., Moene, A.F., Molinos, F., Moulin, E., Pietersen, H.P., Piguet, B., Pique, E., Román-Cascón, C., Rufin-Soler, C., Saïd, F., Sastre-Marugán, M., Seity, Y., Steeneveld, G.J., Toscano, P., Traullé, O., Tzanos, D., Wacker, S., Wildmann, N., Zaldei, A., 2014. The BLLAST field experiment: boundary-layer late afternoon and sunset turbulence. Atmos. Chem. Phys. 14 (10), 931–960. https://doi.org/10.5194/acp-14-10931-2014.
Manninen, A.J., 2019a. Developing Methods for Doppler Lidar to Investigate Atmospheric Boundary Layer. University of Helsinki [online] Available from: urn:ISBN:978–952-7276-19-8.
Manninen, A.J., 2019b. Halo Lidar Toolbox, Github [online] Available from. https://github.com/manninenaj/HALO_lidar_toolbox.
Manninen, A.J., O'Connor, E.J., Vakkari, V., Petäjä, T., 2016. A generalised background correction algorithm for a Halo Doppler lidar and its application to data from Finland. Atmos. Meas. Tech. 9 (2), 817–827. https://doi.org/10.5194/amt-9-817-2016.
Manninen, A.J., Marke, T., Tuononen, M., O'Connor, E.J., 2018. Atmospheric boundary layer classification with Doppler lidar. J. Geophys. Res. Atmos. 123, 8172–8189. https://doi.org/10.1029/2017JD028169.
Moya, M.R., López-Ballesteros, A., Sánchez-Cañete, E.P., Serrano-Ortiz, P., Oyonarte, C., Domingo, F., Kowalski, A.S., 2022. Ecosystem CO2 release driven by wind occurs in drylands at global scale. Glob. Chang. Biol. 00, 1–14. https://doi.org/10.1111/gcb.16277.
Nachshon, U., Dragila, M., Weisbrod, N., 2012. From atmospheric winds to fracture ventilation: cause and effect. J. Geophys. Res. Biogeosci. 117 (2) https://doi.org/10.1029/2011JG001898.
Newsom, R.K., Alan Brewer, W., Wilczak, J.M., Wolfe, D.E., Oncley, S.P., Lundquist, J.K., 2017. Validating precision estimates in horizontal wind measurements from a Doppler lidar. Atmos. Meas. Tech. 10, 1229–1240. https://doi.org/10.5194/amt-10-1229-2017.
O'Connor, E.J., Illingworth, A.J., Brooks, I.M., Westbrook, C.D., Hogan, R.J., Davies, F., Brooks, A.B.J., 2010. A method for estimating the turbulent kinetic energy dissipation rate from a vertically pointing doppler lidar, and independent evaluation from balloon-borne in situ measurements. J. Atmos. Ocean. Technol. 27, 1652–1664. https://doi.org/10.1175/2010JTECHA1455.1.
Oke, T.R., 1992. Boundary Layer Climates, Second ed. Routledge, London.
Ortiz-Amezcua, P., Martínez-Herrera, A., Manninen, A.J., Pentikäinen, P., O'Connor, E. J., Guerrero-Rascado, J.L., Alados-Arboledas, L., 2022. Wind and turbulence statistics in the urban boundary-layer over a mountain-valley system in Granada, Spain. Remote Sens. 14 (10), 2321. https://doi.org/10.3390/rs14102321.
Paquin, J.E., Pond, S., 1971. The determination of the Kolmogoroff constants for velocity, temperature and humidity fluctuations from second-and third-order structure functions. J. Fluid Mech. 50 (2), 257–269. https://doi.org/10.1017/S0022112071002568.
Päschke, E., Leinweber, R., Lehmann, V., 2015. An assessment of the performance of a 1.5 μm Doppler lidar for operational vertical wind profiling based on a 1-year trial. Atmos. Meas. Tech. 8, 22151–22266. https://doi.org/10.5194/amt-8-2251-2015.
Pentikäinen, P., James O'connor, E., Manninen, A.J., Ortiz-Amezcua, P., 2020. Methodology for deriving the telescope focus function and its uncertainty for a heterodyne pulsed Doppler lidar. Atmos. Meas. Tech. 13 (5), 2849–2863. https://doi.org/10.5194/amt-13-2849-2020.
Rastogi, A., Stróżecki, M., Kalaji, H.M., Łuców, D., Lamentowicz, M., Juszczak, R., 2019. Impact of warming and reduced precipitation on photosynthetic and remote sensing properties of peatland vegetation. Environ. Exp. Bot. 160 https://doi.org/10.1016/j.envexpbot.2019.01.005.
Rey, A., Belelli-Marchesini, L., Were, A., Serrano-ortiz, P., Etiope, G., Papale, D., Domingo, F., Pegoraro, E., 2012. Wind as a main driver of the net ecosystem carbon balance of a semiarid Mediterranean steppe in the South East of Spain. Glob. Chang. Biol. 18 (2), 539–554. https://doi.org/10.1111/j.1365-2486.2011.02534.x.
Rimoldini, L., 2014. Weighted skewness and kurtosis unbiased by sample size and Gaussian uncertainties. Astron. Comput. 5, 1–8. https://doi.org/10.1016/j.ascom.2014.02.001.
Rojo, J., Rapp, A., Lara, B., Fernández-González, F., Pérez-Badia, R., 2015. Effect of land uses and wind direction on the contribution of local sources to airborne pollen. Sci. Total Environ. 538, 672–682. https://doi.org/10.1016/J.SCITOTENV.2015.08.074.
Sánchez-Cañete, E.P., Oyonarte, C., Serrano-Ortiz, P., Curiel Yuste, J., Pérez-Priego, O., Domingo, F., Kowalski, A.S., 2016. Winds induce CO2 exchange with the atmosphere and vadose zone transport in a karstic ecosystem. J. Geophys. Res. Biogeosci. 121 (8) https://doi.org/10.1002/2016JG003500.
Vakkari, V., Manninen, A.J., O'Connor, E.J., Schween, J.H., Van Zyl, P.G., Marinou, E., 2019. A novel post-processing algorithm for Halo Doppler lidars. Atmos. Meas. Tech. 12 (2), 839–852. https://doi.org/10.5194/amt-12-839-2019.
Vicente-Vicente, J.L., García-Ruiz, R., Francaviglia, R., Aguilera, E., Smith, P., 2016. Soil carbon sequestration rates under Mediterranean woody crops using recommended management practices: a meta-analysis. Agric. Ecosyst. Environ. 235, 204–214. https://doi.org/10.1016/J.AGEE.2016.10.024.
Wood, R., 2012. Stratocumulus clouds. Mon. Weather Rev. 140 (8), 2373–2423. https://doi.org/10.1175/MWR-D-11-00121.1.